AIAA Aviation
22-26 June 2015, Dallas, TX
AIAA Modeling and Simulation Technologies Conference

Modeling and Control of Tethered Unmanned Multicopters in Hovering Flight

Davi Ferreira de Castro*, Jônatas Sant'Anna Santos†, Marco Batista Xandó de Oliveira‡, Davi Antônio dos Santos§ and Luiz Carlos Sandoval Góes¶

Instituto Tecnológico de Aeronáutica, São José dos Campos, São Paulo, 12228-900, Brasil

The dynamic modeling, navigation and control for free-flying Robots are greatly discussed topics in the scientific community. On the other hand, implications on tethered flights are rarely approached. This paper presents a modeling and control strategy for tethered unmanned multicopters. A viscoelastic model is considered for the cable, in order to reproduce its dynamic behavior. A control strategy is presented for hovering tethered multicopter and a comparison between free and tethered flight using an unmanned multicopter is presented.

Nomenclature

S_{B}	Body system
S_{I}	Inertial system
S_{R}	Reference system
$\mathbf{q}$	Quaternion of rotation
ϕ	Roll, rad
θ	Pitch, rad
ψ	Yaw, rad
$\boldsymbol{\omega}$	Angular velocity, rad/s
$\boldsymbol{\tau}$	Propulsion resulting torque, Nm
f	Total thrust, N
g	Gravitational acceleration, m/s^2
m	Mass, kg
$\mathbf{r}$	Three-dimensional position
$\mathbf{n}$	Normal unit vector perpendicular to the plane
$\mathbf{I}$	Matrix of inertia
m	Mass, kg

I. Introduction

Unmanned aerial vehicles (UAVs) have been the subject of many academic studies and have attracted a lot of attention from industry in recent years. While in the past the applications were restricted to the defense sector, today, UAVs have many civilian applications too. Possible applications of these vehicles include search and rescue[1], environmental monitoring[2], building inspection[3], border surveillance[4], fire monitoring[5], monitoring of electric energy transmission lines[6], traffic monitoring[7] and surveillance in urban areas[8]. Basically, there are two main categories of UAVs, viz.,fixed wing and the rotary wing UAVs. Fixed wing UAVs

*PhD Student, ITA Mechanical Engineering Department, davifcastro@gmail.com
†PhD Student, ITA Mechanical Engineering Department, jonatas.santos@altave.com.br
‡PhD Student, ITA Mechanical Engineering Department, marco.batista@altave.com.br
§Professor, ITA Mechanical Engineering Department, davists@ita.br
¶Professor, ITA Mechanical Engineering Department, goes@ita.br

have the advantage of being able to fly at high speeds for longer duration. On the other hand, rotary wing UAVs (also called multicopters) have flight capabilities such as hovering, Vertical Take-Off and Landing (VTOL) and pirouetting with agile maneuvering capability, which cannot be achieved by conventional fixed wing aircraft. However, the power system is embedded, which results in limitated autonomy, and permitting flights of at most an hour.

The multicopter vehicles have become very popular in UAVs research. This interest can be explained by the relatively low cost, smaller size and higher maneuverability, allowing both outdoor and indoor flights. A sub-category of multicopters is tethered multicopters UAVs, which are anchored at a fixed point by a cable. While this limits their motion, but it can also serve as a power line, providing electrical power to the vehicle and enhancing its flight autonomy. Another advantage of this type of vehicle is its greater hovering capability, since it can be more robust to ambient wind, due to the tension exerted by the cable.

In recent years, tethered balloon[9] and tethered robot satellite[10] are quite common. However, there is not much literature available addressing multicopters. A strategy to control a tethered helicopter with a combination of classical PID control laws is provided by Sandino *et al*[11].

The cable provides more robustness against external disturbances due to the stabilizing properties of tether tension in translational dynamics. On the other hand, the tether tension produces an induced moment due to the offset between the point of application of the tension and the center of mass of the vehicle. Since this moment could be similar or larger in magnitide to the torque required to control the rotation of the vehicle in free flight, it must be properly accounted for this undesired rotational influence. This paper presents a modeling and control strategy for tethered unmanned multicopter in hover. Here, the controller is based on a saturated state feedback control, thus simplifying the controller.

This paper is organized as follows. Section II describes a dynamic model corresponding to tethered multicopter. Section III describes a control strategy for hovering. Section IV presents results of simulations, and Section V contains conclusions of this study.

II. Tethered Configuration Model

This section decribes a model corresponding to the tethered configuration. The objective is not to present very elaborate equations for high-fidelity simulations, but to derive the best model for control design purposes.

A. Multicopter Model

Consider a octocopter and three Cartesian coordinate systems (CCS) illustrated in Figure 1. The CCS of the body $S_{\mathrm{B}} \triangleq \{X_{\mathrm{B}},\ Y_{\mathrm{B}},\ Z_{\mathrm{B}}\}$ is fixed to the vehicle structure and centered on the center of mass (CM). The CCS inertial $S_{\mathrm{I}} \triangleq \{X_{\mathrm{I}},\ Y_{\mathrm{I}},\ Z_{\mathrm{I}}\}$ is fixed to the earth at the point O. The CCS $S_{\mathrm{R}} \triangleq \{X_{\mathrm{R}},\ Y_{\mathrm{R}},\ Z_{\mathrm{R}}\}$ is parallel to S_{I} and centered in CM. $\mathrm{T_C}$ is tether tension and $\mathbf{c}$ defined tether line vector.

The differential equations that describes the dynamic behavior of the multirotor can be obtained by the Newton-Euler formulation. In this study, we choose to represent the attitude by the quaternion of rotation $\mathbf{q} \in \mathbb{R}^4$, however for visualization is adopted Euler angles (ϕ, θ and ψ).

The kinematic attitude model for the quaternion of rotation is given by the following differential equation:[12]

$$\dot{\mathbf{q}} = \mathbf{\Omega}\mathbf{q}, \tag{1}$$

where,

$$\mathbf{\Omega} = \frac{1}{2}\begin{bmatrix} 0 & -\boldsymbol{\omega}^{\mathrm{T}} \\ \boldsymbol{\omega} & -[\boldsymbol{\omega}\times] \end{bmatrix}, \tag{2}$$

being $\boldsymbol{\omega} \triangleq [\omega_x\ \omega_y\ \omega_z]^{\mathrm{T}} \in \mathbb{R}^3$ the angular velocity of the vehicle represented in S_{R} and $[\boldsymbol{\omega}\times]$ is given by:

$$[\boldsymbol{\omega}\times] = \begin{bmatrix} 0 & -\omega_z & \omega_y \\ \omega_z & 0 & -\omega_x \\ -\omega_y & \omega_x & 0 \end{bmatrix}. \tag{3}$$

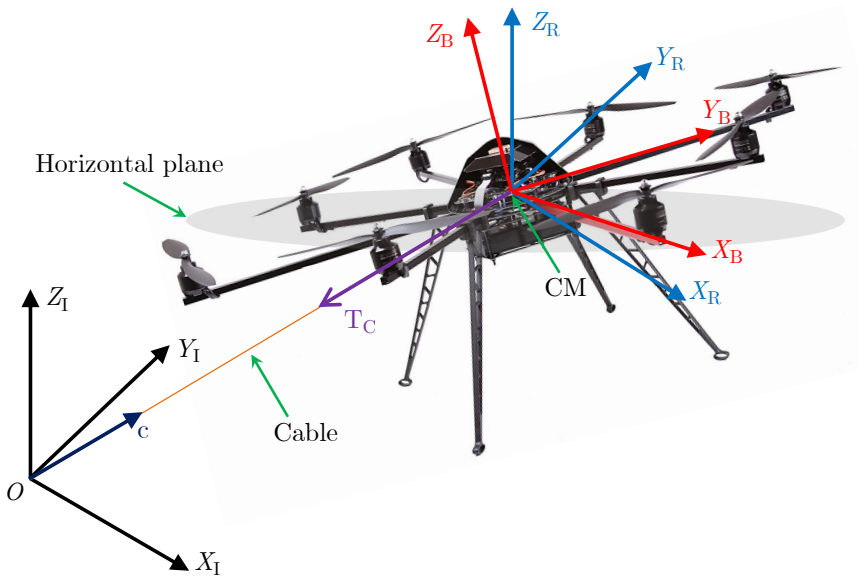

Figure 1. Cartesian coordinate systems.

Rewriting Equation (1) explicitly, one can obtain:

$$\begin{bmatrix} \dot{q}_1 \\ \dot{q}_2 \\ \dot{q}_3 \\ \dot{q}_4 \end{bmatrix} = \frac{1}{2} \begin{bmatrix} 0 & -\omega_x & -\omega_y & -\omega_z \\ \omega_x & 0 & \omega_z & -\omega_y \\ \omega_y & -\omega_z & 0 & \omega_x \\ \omega_z & \omega_y & -\omega_x & 0 \end{bmatrix} \begin{bmatrix} q_1 \\ q_2 \\ q_3 \\ q_4 \end{bmatrix}. \tag{4}$$

Applying Newton's second law for rotational motion and neglecting disturbance torques, one can obtain:

$$\boldsymbol{\tau} = \dot{\mathbf{h}} + \boldsymbol{\omega} \times \mathbf{h}, \tag{5}$$

where $\boldsymbol{\tau} \triangleq [\tau_x \ \tau_y \ \tau_z]^{\mathrm{T}} \in \mathbb{R}^3$ is the propulsion resulting torque in vehicle represented in S_{B} and $\mathbf{h} \triangleq \mathbf{I}\,\boldsymbol{\omega} \in \mathbb{R}^3$ is the angular momentum of the body represented in S_{B}, being $\mathbf{I} \in \mathbb{R}^{3x3}$ the matrix of inertia of the vehicle represented in S_{B}. It is assumed that the vehicle has symmetrical structure with respect to the coordinate axes. The matrix $\mathbf{I}$ resulting in a diagonal matrix defined by:

$$\mathbf{I} = \begin{bmatrix} I_x & 0 & 0 \\ 0 & I_y & 0 \\ 0 & 0 & I_z \end{bmatrix}. \tag{6}$$

Rewriting Equation (5) explicitly, one can obtain:

$$\dot{\omega}_x = \frac{(I_y - I_z)}{I_x}\omega_y\omega_z + \frac{\tau_x}{I_x}. \tag{7}$$

$$\dot{\omega}_y = \frac{(I_z - I_x)}{I_y}\omega_x\omega_z + \frac{\tau_y}{I_y}. \tag{8}$$

$$\dot{\omega}_z = \frac{(I_x - I_y)}{I_z}\omega_x\omega_y + \frac{\tau_z}{I_z}. \tag{9}$$

Applying the Newton's second law of motion and neglecting any perturbations, one can obtain the following model of translational movement S_{I}:

$$\ddot{\mathbf{r}} = \frac{1}{m} f \mathbf{n} + \begin{bmatrix} 0 \\ 0 \\ -g \end{bmatrix}, \tag{10}$$

where $\mathbf{r} \triangleq [r_x \; r_y \; r_z]^{\mathrm{T}} \in \mathbb{R}^3$ is the three-dimensional position of the CM represented as S_{I}, $\mathbf{n} \triangleq [n_x \; n_y \; n_z]^{\mathrm{T}} \in \mathbb{R}^3$ is the normal unit vector perpendicular to the rotor plane represented as S_{I}, f is the total thrust magnitude, g is the gravitational acceleration and m is the mass of the vehicle.

B. Tether Model

A viscoelastic model for the cable is considered in order to reproduce its behavior, as illustrated in Figure 2. More precisely, the model consists of a damper with coefficient d_a and a spring with stiffness k_a in parallel, both connected in series with a spring of different stiffness k_b.

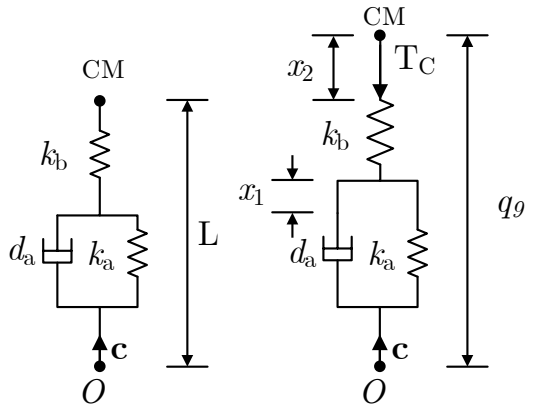

(a) Unstressed tether (b) Elongated tether

Figure 2. Viscoelastic model of the tether.

Where x_1 is an unobservable variable which describes the inner friction, x_2 represents the elongation of that segment, L denotes the unstressed tether segment lenght that is reeled out by the ground device and q_9 is deployed tether segment. It is important to note that in the model adopted the mass of the cable is considered negligible in relation to the vehicle mass. The equations and parameters are proposed by Sandino *et al*[11]. The variables that describe the tether state are shown in Figure 2. The transfer function associated tether model is proposed by Sandino *et al*[11] is given by:

$$\mathrm{G(s)} = \frac{\mathrm{T_C(s)}}{\mathrm{U_C(s)}} = \frac{d_a k_b \left(\frac{k_a}{d_a} + s \right)}{s(k_a + k_b + d_a s)} \tag{11}$$

where $\mathrm{U_C(s)}$ represents the tether velocity of frequency domain. Regarding model parameters d_a, k_a and k_b, they are usually expressed as:

$$k_a = \frac{q.\mathrm{E}_1}{\mathrm{L}}, \; k_b = \frac{q.\mathrm{E}_2}{\mathrm{L}}, \; d_a = \frac{q.\eta}{\mathrm{L}} \tag{12}$$

Parameter values that have been used in this study for simulation purposes are listed in Table 1.

III. Control Strategy

The control strategy focusses on three approaches, viz., cable tension, multicopter, and tethered multicopter, respectively.

Table 1. Parameters of the tether model[11].

	Parameter	Value	Units
Diameter	d_C	$10e^{-3}$	m
Cross section	q	$\pi\left(\frac{d_C}{2}\right)^2$	m^2
Modulus of elasticity	E_1	0.194	GPa
	E_1	0.543	GPa
Viscosity	η	0.096	GPa.s
Initial tether length	L_0	10	m

A. Tether Control

The tether tension is controlled by a proportional control configuration. The Equation 13 and Figure 3 show the architecture of the tether control, which is described by Sandino *et al*[11].

$$U_C{}^\star = k_p(T_C{}^\star - T_C) \tag{13}$$

where $U_C{}^\star$ is the desired velocity tether, $T_C{}^\star$ is the desired tether tension and k_p is proportional gain.

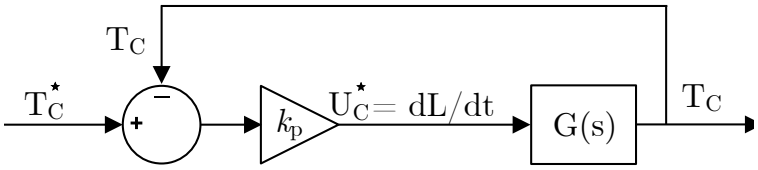

Figure 3. Control system for simplified tether model given by G(s) is proposed by Sandino *et al*[11].

B. Multicopter Control

The multicopter control strategy presented in this section is described by Santos *et al*[13]. Let us define the total thrust vector $\in \mathbb{R}^3$ of the octocopter to be:

$$\mathbf{f} \triangleq f\mathbf{n}. \tag{14}$$

Let us define the inclination angle $\varphi \in \mathbb{R}$ of the octocopter to be:

$$\varphi \triangleq \cos^{-1} n_z. \tag{15}$$

Note that φ consists of the angle between $\mathbf{n}$ and Z_R (see Figure 4).

Let $\overline{\mathbf{r}} \triangleq [\overline{r}_x\ \overline{r}_y\ \overline{r}_z]^T \in \mathbb{R}^3$ denote the position desired for the octocopter and define the corresponding tracking error $\tilde{\mathbf{r}}^{(i)} \in \mathbb{R}^3$ by

$$\tilde{\mathbf{r}} \triangleq \mathbf{r} - \overline{\mathbf{r}}. \tag{16}$$

Let $\varphi_{max} \in \mathbb{R}$ be the maximum allowable values of the inclination angle φ, $f_{min} \in \mathbb{R}$ and $f_{max} \in \mathbb{R}$ be, respectively, the minimum and the maximum allowable values of the total thrust magnitude f. The solution to the problem of position control is to find a feedback control law for $\mathbf{f}$, which make $\mathbf{r} \to \overline{\mathbf{r}}$ or $\tilde{\mathbf{r}} \to \mathbf{0}$, while respecting the constraints $f_{min} \leq f \leq f_{max}$ and $\varphi \leq \varphi_{max}$. The control position is partitioned into control height and horizontal position control.

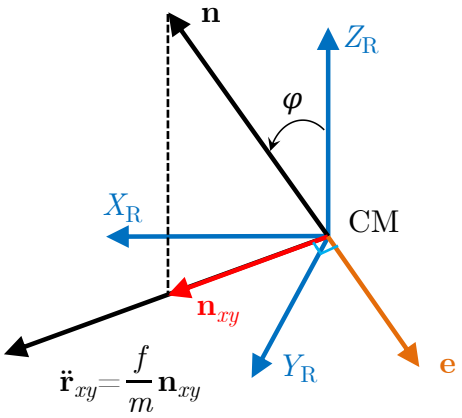

Figure 4. Relationship between the normal unit vector n and the horizontal acceleration $\ddot{\mathbf{r}}_{xy}$.

1. *Height Control*

From Equation (10), the dynamic model of the height of the vehicle r_z is given by

$$\ddot{r}_z = \frac{n_z}{m} f - g. \tag{17}$$

Consider the system modeled by Equation (17), and the minimum $f_{\min} > 0$ and maximum $f_{\max} > f_{\min}$ allowable values of the command total thrust magnitude f. Assume that m, g and $n_z \neq 0$ are exactly known. The feedback control law is given by:

$$f = \begin{cases} f_{\min}, & \alpha_z < f_{\min} \\ \alpha_z, & \alpha_z \in [f_{\min}, f_{\max}] \\ f_{\max}, & \alpha_z > f_{\max} \end{cases} \tag{18}$$

with

$$\alpha_z \triangleq \frac{m}{n_z} \left(g - k_1 \left(r_z - r_{\mathrm{z}} \right) - k_2 \dot{r}_z \right), \tag{19}$$

respecting the total thrust magnitude constraint $f_{\min} \leq f \leq f_{\max}$ and is such that if $f_{\min} \leq \alpha_z \leq f_{\max}$, then the vehicle height r_z responds to the height desired $\overline{r}_z$, as if it were governed by the following second order linear time-invariant (LTI) system:

$$\ddot{r}_z + k_2 \dot{r}_z + k_1 r_z = k_1 \overline{r}_z, \tag{20}$$

where $k_1 > 0 \in \mathbb{R}$ e $k_2 > 0 \in \mathbb{R}$ are controller coefficients.

2. *Horizontal Position Control*

Let $\mathbf{r}_{xy} \triangleq [r_x \; r_y]^{\mathrm{T}} \in \mathbb{R}^2$ and $\mathbf{n}_{xy} \triangleq [n_x \; n_y]^{\mathrm{T}} \in \mathbb{R}^2$ denote the horizontal projections of $\mathbf{r}$ and $\mathbf{n}$, respectively. From equation (10), one can write the horizon position dynamic model as

$$\ddot{\mathbf{r}}_{xy} = \frac{f}{m} \mathbf{n}_{xy}. \tag{21}$$

Consider the system modeled by equation (21) and the maximum allowable value $\varphi_{\max} > 0$ of the inclination angle φ. Assume that m and $f \neq 0$ are exactly known. The feedback control law is given by:

$$\mathbf{n}_{xy} = \begin{cases} \boldsymbol{\alpha}_{xy}, & \|\boldsymbol{\alpha}_{xy}\| \leq \sin \varphi_{\max} \\ \sin \varphi_{\max} \frac{\boldsymbol{\alpha}_{xy}}{\|\boldsymbol{\alpha}_{xy}\|}, & \|\boldsymbol{\alpha}_{xy}\| > \sin \varphi_{\max} \end{cases}, \tag{22}$$

with

$$\boldsymbol{\alpha}_{xy} \triangleq -\frac{m}{f}\left[k_z\left(\mathbf{r}_{xy}-\mathbf{r}_{xy}\right)+k_4\dot{\mathbf{r}}_{xy}\right], \tag{23}$$

respecting the inclination angle constraint $\varphi \leq \varphi_{\max}$ and is such that if $\|\boldsymbol{\alpha}_{xy}\| \leq \sin\varphi_{\max}$, then $\mathbf{r}_{xy}$ responds to the horizontal position desired $\overline{\mathbf{r}}_{xy} \triangleq [\overline{r}_x\ \overline{r}_y]^{\mathrm{T}}$ as if it were governed by the following pair of second order LTI systems:

$$\ddot{\mathbf{r}}_{xy}+k_4\dot{\mathbf{r}}_{xy}+k_3\mathbf{r}_{xy}=k_3\overline{\mathbf{r}}_{xy}, \tag{24}$$

where $k_3>0\in\mathbb{R}$ e $k_4>0\in\mathbb{R}$ are controller coefficients.

In practice, the attitude desired for the internal attitude control loops need to be computed from the normal unit vectors $\mathbf{n}$. In order to specify a unique attitude, it is necessary to select a heading. For example, one can choose a zero heading just by taking into consideration the attitude represented by the principal Euler angle/axis $(\varphi,\mathbf{e})$, where φ is the angle of inclination own and $\mathbf{e}\in\mathbb{R}^3$ is a unit vector (see Figure 4) is given by:

$$\mathbf{e}=\frac{\mathbf{n}\times\mathbf{n}_{xy}}{\|\mathbf{n}\times\mathbf{n}_{xy}\|} \tag{25}$$

From $(\varphi,\mathbf{e})$ one can thus represent the attitude of S_{B} with respect to S_{R}, using , for example, Euler angles parameterization that permits obtains $\overline{\phi}$, $\overline{\theta}$ and $\overline{\psi}$.

C. Tethered Multicopter Control

In order to control the height, a term $\mathrm{T_C}$ was added in Equation23. Therefore, Equation 26 represents the proposed controller.

$$\alpha_z \triangleq \frac{m}{n_z}\left(g-k_1\left(r_z-r_{\mathrm{z}}\right)-k_2\dot{r}_z\right)+\mathrm{T_C} \tag{26}$$

IV. Simulation Results

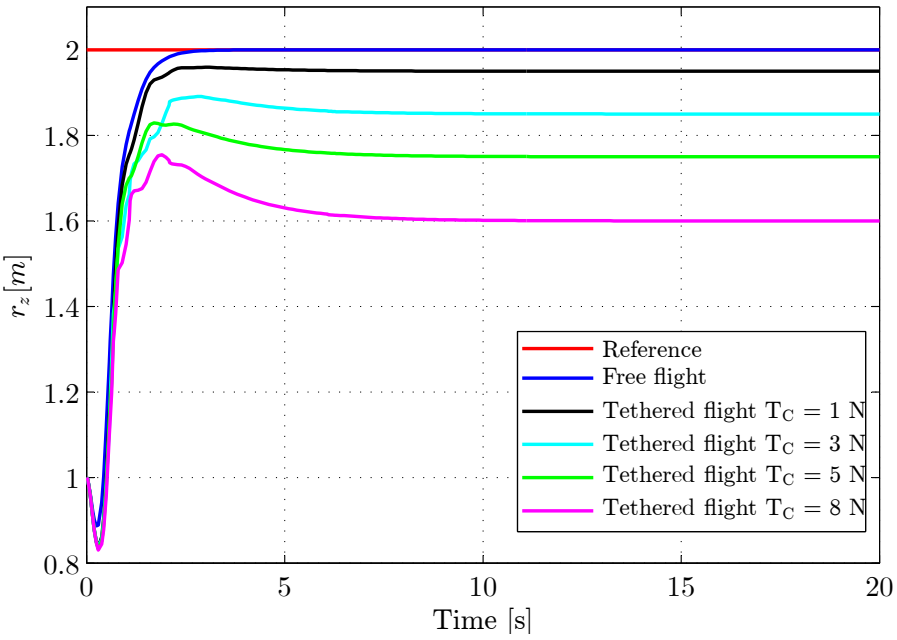

Figure 5. Comparisons between free and tethered flight using the multicopter controller.

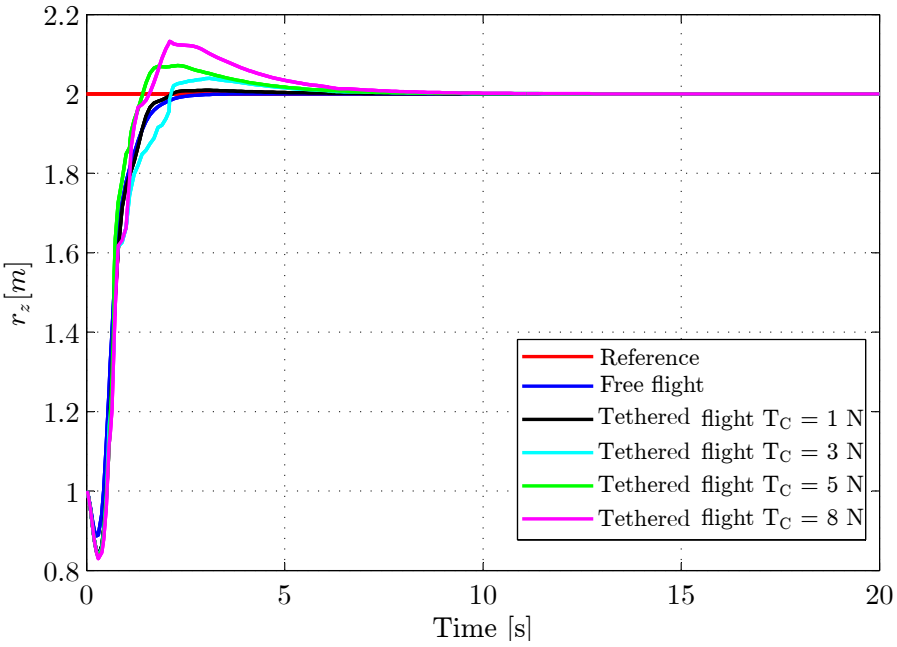

Figure 6. Comparisons between free and tethered flight using the tethered multicopter controller.

The multicopter dynamics is integrated by using the fourth order Runge-Kutta method with time step of $T = 0.002$ s. The initial position is: $\mathbf{r} = [0\ 0\ 1]^{\mathrm{T}}$m. The mass of vehicle is $m = 2.132$ kg and the gravity acceleration is $g = 9.796$ m/s^2. The control parameters of vehicle, k_1, k_2, k_3 and k_4, are chosen based on equations (20) and (24). The maximum overshoot of $M_{\mathrm{p}}^{\mathrm{ref}} = 0.02$ m, and a peak time of $t_{\mathrm{p}}^{\mathrm{ref}} = 2$ s, were selected, which resulted in $k_1 = 6.29$ and $k_2 = 3.91$. Similarly, the maximum overshoot of $M_{\mathrm{p}}^{\mathrm{ref}} = 0.02$ m and a peak time of $t_{\mathrm{p}}^{\mathrm{ref}} = 3$ s were selected and the $k_3 = 2.78$ and $k_4 = 2.61$ gains were obtained. The proportional gain tether control selected was $k_p = 0.01$. The simulation was ran for 20 seconds, and the following bounds were selected: $\varphi_{max} = 30°$, $f_{max} = 40$ N e $f_{min} = 2$ N. These parameters were used by Castro[14].

The simulations provide comparisons between free and tethered flight. Four tethered flight simulations were performed and the tether tension were 1,3,5 and 8 N, respectively. The aim was to track a height of 2 m, as shown by the reference line in Figure 5

The Multicopter Controller was used in the first simulation and the modification proposed in the Tethered Multicopter Controller was used in the second simulation.

Figure 5 shows that the Multicopter Controller did not follow the reference in the tethered flights and the error increased with increase in the tether tension.

Figure 6 shows that it is possible to follow the reference using the tethered multicopter controller.

V. Conclusions

The key achievement of this paper was to confirm the possibility of maintaining a fixed tension in the cable in a tethered flight using unmanned multicopters. The simulation results proved the effectiveness of the Tethered Multicopter Controller proposed in this paper. Further it is seen by the simulations that it is possible to fly with increasing the tether tension, ensuring some level of autonomy in hovering flights. This system is useful to have high autonomy in operation and ability to maintain the cable tensioned during the flight.

Acknowledgments

The authors would like to thank CAPES, CNPq and FAPEAM, Brazil, for financial support to carry out this research project. We would also like to thank ALTAVE LTDA., and its founders Bruno Avena and Leonardo Nogueira for partnership in conducting this research.

References

[1]Tomić, T., Schmid, K., Lutz, P., Domel, A., Kassecker, M., Mair, E., Grixa, I. L., Ruess, F., Suppa, M., and Burschka, D., "Toward a Fully Autonomous UAV : Research Platform for Indoor and Outdoor Urban Search and Rescue," *IEEE Robotics and Automation Magazine*, 2012.

[2]Koo, V. C., Chan, Y. K., Gobi, V., Chua, M. Y., Lim, C. H., Lim, C. S., Thum, C. C., Lim, T. S., Ahmad, Z., Mahmood, K. A., Shahid, M. H., Ang, C. Y., Tan, W. Q., Tan, P. N., Yee1, K. S., Cheaw, W. G., Boey, H. S., Choo, A. L., and Sew, B. C., "A New Unmanned Aerial Vehicle Synthetic Aperture Radar for Environmental Monitoring," *Progress In Electromagnetics Research*, Vol. 122, 2012, pp. 245–268.

[3]Eschmann, C., KUO, C. M., KUO, C. H., and BOLLER, C., "Unmanned Aircraft Systems for Remote Building Inspection and Monitoring," *6th European Workshop on Structural Health Monitoring, Dresden, Germany*, 2012.

[4]Girard, A. R., Howell, A. S., and Hedrick, J. K., "Border Patrol and Surveillance Missions using Multiple Unmanned Air Vehicles," *43rd IEEE Conference on Decision and Control, Atlantis, Paradise Island, Bahamas*, 2004.

[5]Casbeer, D. W., Li, S.-M., Beard, R. W., Mehra, R. K., and McLain, T. W., "Forest Fire Monitoring With Multiple Small UAVs," *American Control Conference, Portland, OR, USA*, 2005.

[6]Li, Z., Li, Y., Walker, R., Hayward, R., and Zhang, J., "Towards Automatic Power Line Detection for a UAV Surveillance System Using Pulse Coupled Neural Filter and an Improved Hough Transform," *Machine Vision and Applications*, Vol. 21, 2010, pp. 677–686.

[7]Puri, A., Valavanis, K. P., and Kontitsis, M., "Statistical Profile Generation for Traffic Monitoring Using Real-time UAV based Video Data," *Mediterranean Conference on Control and Automation, Athens, Greece*, 2007, pp. 1–6.

[8]Semsch, E., Jakob, M., Pavlicek, D., and Pechoucek, M., "Autonomous UAV Surveillance in Complex Urban Environments," *IEEE/WIC/ACM International Conference on Web Intelligence and Intelligent Agent Technology*, 2009, pp. 82–85.

[9]Khaleefa, S., Alsamhi, S., and Rajput, N., "Tethered balloon technology for telecommunication, coverage and path loss," *Electrical, Electronics and Computer Science (SCEECS)*, 2014.

[10]Nohmi, M., "Mission Design of a Tethered Robot Satellite STARS for Orbital Experiment," *18th IEEE International Conference on Control Applications*, Saint Petersburg, Russia, 2009.

[11]Sandino, L. A., Bejar, M., Kondak, K., and Ollero, A., "Advances in Modeling and Control of Tethered Unmanned Helicopters to Enhance Hovering Performance," *Journal of Intelligent and Robotic Systems*, Vol. 73, 2014, pp. 3–18.

[12]Wertz, J. R., *Spacecraft Attitude Determination and control*, Kluwer Academic Publishers, The Netherlands, 1978.

[13]Santos, D. A., Saotome, O., and Cela, A., "Position Formation Control of Multirotors using Thrust Vector Constraints," *IEEE Transactions on Aerospace and Electronic Systems*, 2013.

[14]Castro, D. F., *Ambiente de Simulacao SIL para Sistemas de Controle de Formacao em Posicao para Multicopteros*, Mestrado em engenharia mecanica, Instituto Tecnologico de Aeronautica, Dezembro 2014.